Metal-free design of a multilayered metamaterial with chirped Bragg grating for enhanced radiative cooling: supplement

D. OSUNA RUIZ,[1,*] C. LEZAUN,[1] A. E. TORRES-GARCÍA,[1] AND M. BERUETE[1,2,3]

[1]*Department of Electrical, Electronic and Communications Engineering, Public University of Navarra, 31006 Pamplona, Spain*
[2]*Institute of Smart Cities (ISC), 31006 Pamplona, Spain*
[3]*miguel.beruete@unavarra.es*
[*]*david.osuna@unavarra.es*

CONTENTS

1. CALCULATIONS USING COUPLED MODE THEORY

In the manuscript, reflectance (R) at normal incidence from calculations performed by the numerical software GD-Calc$^{\text{TM}}$ on a ML with high index-contrast materials was shown. In this section we show that identical results can be obtained using a full analytical method based on coupled mode theory (CMT) using the Transfer Matrix Method equations from ref. [1]. Fig. S1(a) (red open circles) shows R as a function of wavelength (λ) for a ML model with $N = 15$ and $\lambda_1 = 3.1$ µm, using CMT and an infinitely thick SiO$_2$ substrate (implying $T \sim 0$, given material losses and its infinite electrical size), up to 30 µm. Results from GD-Calc$^{\text{TM}}$ for the same ML are overlaid (red solid curve) for the sake of comparison. Both results, either calculating R from GD-Calc$^{\text{TM}}$ or using CMT, have an excellent match. Note that, in the CMT method the substrate is infinitely thick while in GD-Calc$^{\text{TM}}$ is 0.5 mm thick. However, both methods yield the same results for the same materials, which suggests that the substrate finiteness is not affecting R whatsoever. Results are indistinguishable using either method and the reflection bandwidth (BW) is significantly unaltered, which highlights the robustness of the calculated R.

Nonetheless, to test the influence of the substrate on R, Fig. S1(b) shows the reflectivity (r) at the interface between a semi-infinite layer of the SiO$_2$ model and a Al$_2$O$_3$ model (black curve) as the substrate, as a function of λ. Reflectivity is calculated as $r = [(n_{sb} - n_1)/(n_{sb} + n_1)]^2$, where n_{sb} is the substrate index of refraction and n_1 is that of Al$_2$O$_3$ (first layer in the ML). Reflectivity (r) increases at certain wavelengths given the larger index contrast at the interface. Fig. S1(c) shows a comparison between both methods using Al$_2$O$_3$ as the substrate layer. As mentioned above, there are no significant differences between both methods. Besides, as expected from r at the substrate interface, the high-R regions at longer λ appear very close to the locations where r between SiO2$_2$ and Al$_2$O$_3$ is larger. These results reveal that 'undesired' R at the substrate interface is in fact occurring, in addition to other interferences in the ML. The matching with r is not exact precisely because of the latter. Nevertheless, these effects do not alter the reflection performance in the solar window.
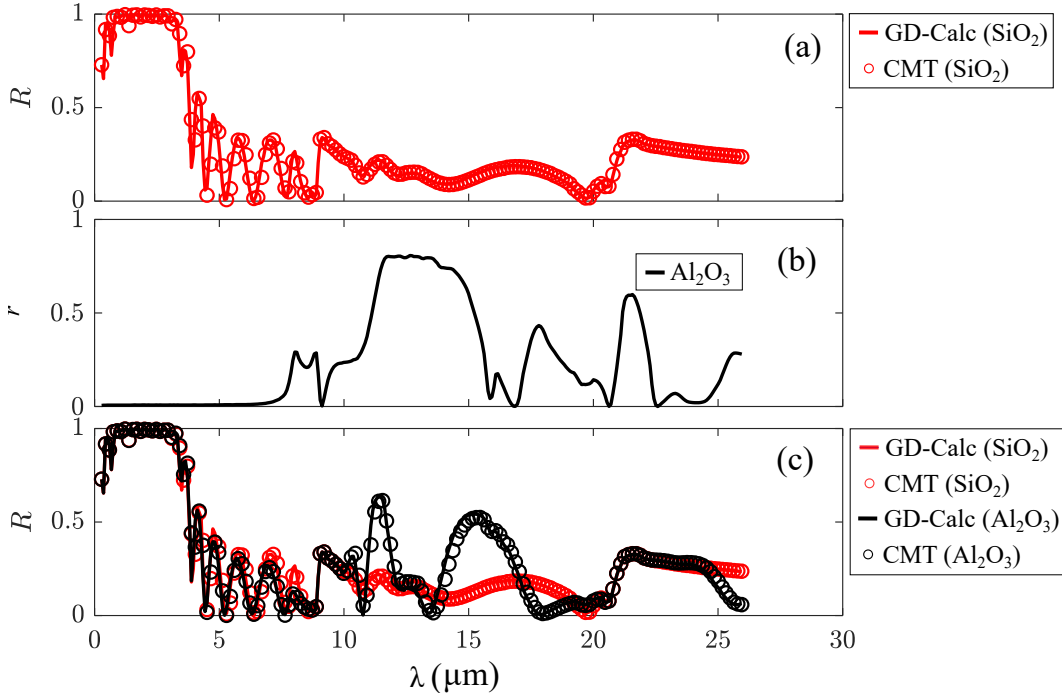
Fig. S1. (a) Simulated R with GD-Calc$^{\text{TM}}$ (solid curve) and calculated with CMT (open circles) using SiO$_2$ as substrate. (b) Reflectivity r at the substrate interface if Al$_2$O$_3$ is used as substrate (black curve). (c) Simulated (solid curve) and calculated (open circles) R when SiO$_2$ or Al$_2$O$_3$ is used as substrate (red and black curves, respectively).

2. MATERIAL PROPERTIES AND MODELS

Fig. S2 shows the optical parameters, index of refraction (n) and the extinction coefficient (κ), of some exemplary materials at our disposal, such as TiO_2, SiO_2, MgF_2 and Si. Some of these models were used in our investigations, as it will be explained later in this same section. The data were obtained from the optical material database from ref. [**?**], downloadable along with the cited software installation package. Note that the (complex) dielectric permittivity ($\epsilon = \epsilon' - i\epsilon''$, where minus sign is set as for common convention) is $\tilde{n}^2$, being $\tilde{n} = n + i\kappa$. We take magnetic relative permeability as unity in all models.
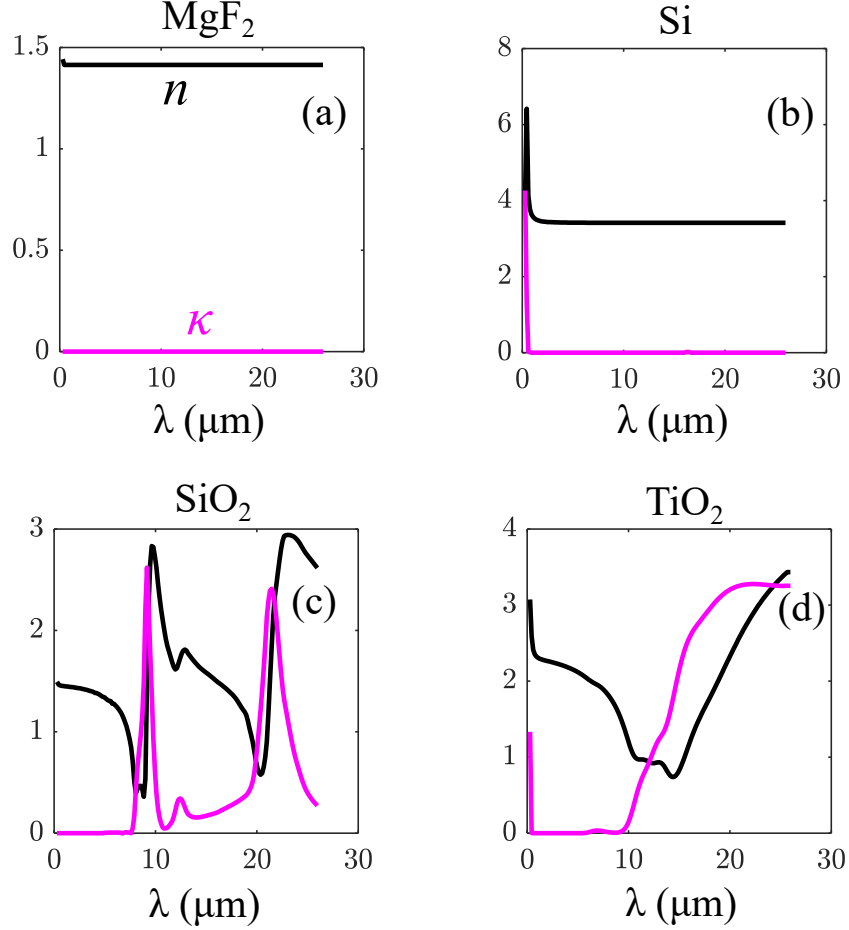
Fig. S2. Index of refraction (n) and extinction coefficient (κ) for the employed material models of (a) MgF_2, (b) Si, (c) SiO_2 and (d) TiO_2, as functions of wavelength (λ) up to 28 µm.

   In the manuscript, we investigate 'Chirped Bragg gratings' made of material models that show a high-index contrast. To that purpose and in order to obtain quantitative results, we chose the material models of SiO_2 and Si to fulfill that condition in our simulations (see Fig. 2(b-c)). In this section we would like to explain the reasons of why choosing such material models, compared to typical SiO_2 and TiO_2, and introduce some relevant fabrication aspects. Also if other materials were used instead, such as MgF_2. Note that further research on fabrication procedures is out of the scope of this work.

   Silicon (Si) and silicon dioxide (SiO_2) are commonly used materials in the fabrication of electronic and photonic devices due to their excellent mechanical, electrical, and optical properties. The heavily contrasted refractive indices of Si and SiO_2, along with the versatility of fabrication methods, have enabled the development of Silicon on Insulator (SOI) technologies which are the base of the current nanoscale photonic advances [2]. Furthermore, the SiO_2/Si multilayer is a well-studied combination that finds diverse applications including all-dielectric mirrors [3], resonant cavity photodetectors [4], bandpass filters [5], polarizers [6] and solar cells [7]. The

choice of fabrication method for Si-SiO$_2$ layers depends on several factors, including the desired film thickness, uniformity, and the specific application of the multilayer. Different techniques such as Physical Vapor Deposition (PVD), Chemical Vapor Deposition (CVD), Atomic Layer Deposition (ALD), E-beam evaporation [8] and Sol-Gel can be employed. Each technique presents distinct advantages and limitations, and selecting the appropriate method is crucial to achieving the desired film quality and properties. Recently, amorphous Si/SiO$_2$ distributed Bragg reflectors have been fabricated with transfer printed single-crystalline Si nanomembranes. This fabrication approach is expected to reduce the process complexity, cost, and lead to the fabrication of large-area, high-performance Si/SiO$_2$-based DBRs [9].

The use of other materials of similar optical properties in the solar window as SiO$_2$, such as MgF$_2$, was also investigated. Nevertheless, the use of this material might be disadvantageous regarding fabrication. MgF$_2$ has typically been used as the 'low-index' material in optical ML structures [10] and, together with Si, both satisfy a considerably high index contrast. MgF$_2$ can be satisfactorily deposited as thin layers (from 20 nm to 1 µm) onto sufficiently heated quartz substrates [10]. However, other practical aspects such as mechanical stress, porosity, adjacent deposition incompatibility and/or cracking may result in a malfunctioning MgF$_2$/Si ML [10–12], via a reflection reduction or less efficient material packing. All these aspects should be carefully considered in case of replacing SiO$_2$ by another material.

In this section, the aim is not to validate fabrication pathways via simulations but rather to show the feasability of devising Bragg MLs using higher contrast-index materials (for example, SiO$_2$ and Si models). We explore the response from an equivalent, lower index contrast ML ($N = 15$) using TiO$_2$ and SiO$_2$ instead. The shortest and longest sections are designed 'ad-hoc' to cover the desired BW, (from 0.3 µm to 3.1 µm). For this, the thicknesses of the SiO$_2$ layers are kept the same as those from the equivalent 'low index material' layers ($i = 1$), and only the TiO$_2$ layers thicknesses are varied to satisfy the Bragg condition. Note that other criteria are as valid as the chosen one as long as the Bragg condition is fulfilled. The chosen criterion yields thicknesses for the TiO$_2$ layers in the first and last sections of $d_1 = 0.137$ µm, and $d_N = 0.027$ µm. Using a higher index material ($i = 2$) instead of TiO$_2$ implies that layers can be thinner in order to cover the longest λ in the BW (for instance, using the model Si, $d_1 = 0.088$ µm for reaching $\lambda_1 = 3.1$ µm).

Fig. S3 shows R as a function of λ, from an equivalent TiO$_2$ and SiO$_2$ ML, and the original ML (where material models of Si and SiO$_2$ were used in simulations instead). Both BWs end at the expected $\lambda_1 = 3.1$ µm. However, given the smaller index contrast between TiO$_2$ and SiO$_2$ for the same N, this combination leads to a smaller reflection in the targeted BW. Adding more sections ($N = 30$) helps to flatten the BW. After a considerable increment of N, R is noticeably increased but also leads to a thicker ML structure. Hence, the overall improvement in R and the ML thickness by using instead higher index-contrast materials, is clear.
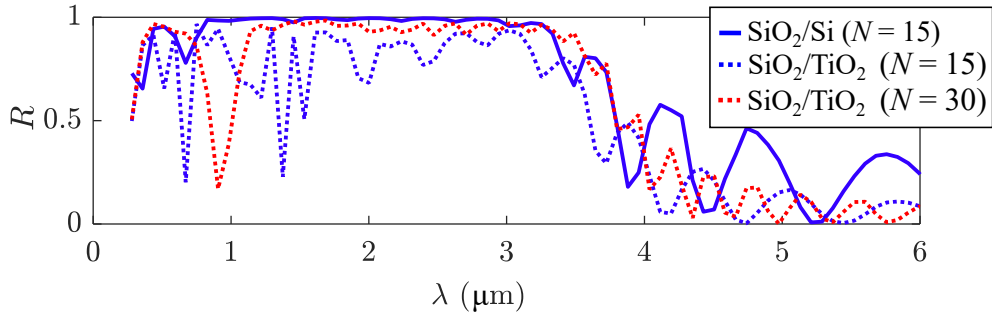
Fig. S3. Simulated R for the original ML from the main text (MgF$_2$ and Si), with $\lambda_1 = 3.1$ µm, for $N = 15$ (solid blue curve), and when Si is replaced by TiO$_2$ and the thicknesses adjusted accordingly to still meet the same Bragg conditions for $N = 15$ (dotted blue curve) and for $N = 30$ (dotted red curve).

Regarding the latter discussion, we must stress that our proposed synthesis process based on a linear chirping, when directly applied *on physical thicknesses only* (as in $d_{i,k} = d_{i,N} + (N - k)(d_{i,1} - d_{i,N})/(N - 1)$), generally assumes that refraction indices ($n_{i,k}$) are practically constant in frequency (i.e., non-dispersive materials). In that case, if the linear chirp is applied on thicknesses directly, regardless of n, the Bragg formula is still satisfied as $n_{i,k}$ are constants with λ. However, if

materials with greater dispersion are used, calculation of $d_{i,k}$ requires to account for $n_{i,k} = n_i(\lambda_k)$ in the Bragg formula, as it is explained next.

The thicknesses for each section and material ($d_{i,k}$) are obtained from the Bragg condition satisfied for that particular λ_k. For $C < 0$, and since material models are the same for each section, we consider two possible scenarios: (1) If materials show little-to-none dispersion, the Bragg formula can be modified to be recursive as $\lambda_{k-1} = 2(n_1\alpha_k d_{1,k} + n_2\alpha_k d_{2,k})$, where $\alpha_k = \lambda_{k-1}/\lambda_k$ for $2 < k < N$ (note that $k = N$ corresponds to the thinnest section or $\lambda_N = 0.3$ µm, and thus $\alpha_k > 1$). This way, successive change in the Bragg wavelength for each section ($\lambda_{k-1} = \alpha_k\lambda_k$) is directly mapped into the change in layer thicknesses $d_{i,k-1} = \alpha_k d_{i,k}$, down to the bottom of the ML. Thus, after fixing $d_{i,N}$, our MATLAB$^{\text{TM}}$ code automatically yields every $d_{i,k}$ required for each λ_k. (2) If materials show significant dispersion, the Bragg condition should still be met, but now it must be applied to the optical thickness of the layers, accounting for dispersion. Starting from a particular layer in section k, the proportionality factor must include the change in dispersion too and so the Bragg formula for section $k-1$, related to that of section k, must be modified as follows: $\lambda_{k-1} = 2(n_{1,k-1}d_{1,k-1} + n_{2,k-1}d_{2,k-1}) = 2(\alpha_k n_{1,k}d_{1,k} + \alpha_k n_{2,k}d_{2,k})$, where $n_{i,k} = n_i(\lambda_k)$. By directly equating each term to the corresponding one from the right side of the equation, and since $\alpha_k = \lambda_{k-1}/\lambda_k$, the new relation between successive thickness layers is

$$d_{i,k-1} = \frac{\lambda_{k-1}}{\lambda_k} \frac{n_i(\lambda_k)}{n_i(\lambda_{k-1})} d_{i,k} \tag{S1}$$

This way, every layer thickness $d_{i,k}$ can still be retrieved recursively. For instance, given $d_{2,N} = 0.02$ µm, and taking $n_1 = n_{\text{SiO}_2}(\lambda_N) = 1.41$ and $n_2 = n_{\text{Si}}(\lambda_N) = 4.2$, which are now dependent on frequency, the Bragg criterion yields $d_{1,N} = 0.047$ µm. Then, for a linear chirp, the rest of layer thicknesses for sections $k < N$ can be directly calculated from $d_{i,N}$ applying the Bragg formula for each λ_k. It is still possible to retrieve each $d_{i,k}$ following the Bragg criterion by selecting the appropriate $n_{i,k}$ at each λ_k. Nevertheless, the synthesis of the CBG turns out particularised for each section and the *linear character in thickness* in the ML is lost. This is because the *physical thicknesses of the layers* ($d_{i,k}$) are no longer 'linearly chirped', strictly speaking, but rather *the product of index and thickness* ($n_{i,k}d_{i,k}$ or 'optical thicknesses'), according to the Bragg formula. If the thicknesses $d_{i,k}$ were retrieved directly from the linear function at the beginning of this paragraph, the Bragg condition is not necessarily met and there is a clear impact on the flatness of the reflected BW, generally worsening the ML response. On the contrary, a linear chirp can be *directly applied to layer physical thicknesses* if materials show very low dispersion in the considered BW.

Fig. S4 shows the atmospheric transmission and the sun irradiance model curves used in our investigations. They were taken from refs [13] and [14], respectively. The reduction in transmission is due to absorption of power by molecules such as CO, CO_2, O_3 or H_2O.
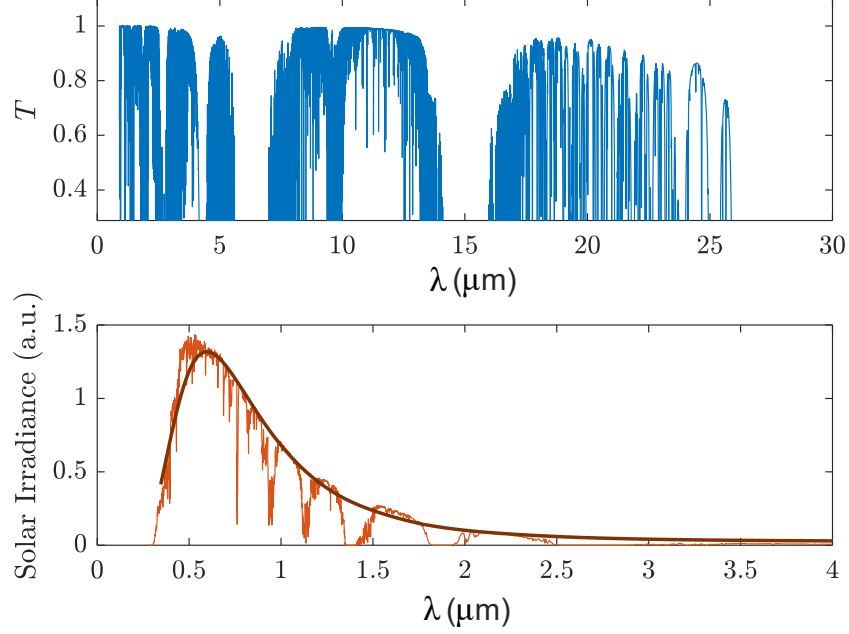
The black body radiation equation,

$$I_{bb}(\lambda) = \frac{2hc^2}{\lambda^5(e^{(hc/\lambda k_b T)} - 1)} \tag{S2}$$

where h is the Planck constant, c is the speed of light in vacuum (in m/s), k_b is the Boltzmann constant and T is the temperature of the object, is overlaid to I model for a temperature of $T = 5778$ K (solid brown curve). From the I model, the fractional power under the curve (as shown in the manuscript) can also be directly calculated by performing a numerical integration following standard methods using MATLAB$^{\text{TM}}$, such as the trapezoidal method.

3. ML WITH A POSITIVE LINEAR CHIRP

We explore here how results are changed when a positive linear chirp ($C > 0$) is applied to the ML layers instead of a negative one. As discussed in the manuscript, the sense of the chirping affects the dispersion properties of the chirped grating [15]. However, our design does not take dispersion into account, and the materials we used have almost negligible losses in the range of wavelengths we explored. Nevertheless, for small wavelengths, the electrical size of the ML would be large and thus small losses may introduce variations, as the dedicated section for such wavelengths would be at the bottom of the structure, as opposed to $C < 0$ (being atop). Fig. S5 shows the R spectrum from a ML similar to the one analyzed in the manuscript for $C < 0$ (solid blue curve) and for $C > 0$ (dotted blue curve) up to 30 µm, with $N = 15$ and $\lambda_1 = 3.1$ µm. In general, the reflected BW (grey shadow) remains significantly unaltered. Only a noticeable

Fig. S4. Model curves for (top panel) atmospheric transmission and (bottom panel) sun irradiance, in arbitrary units, as functions of λ. Black body radiation model for $T = 5778$ K is overlaid to the solar irradiance model.

reduction of R at the lowest end ($\lambda \approx 0.3$ µm) is observed for $C > 0$ using the 'little-to-none losses' material models, as expected. Therefore, a $C > 0$ linear chirp may potentially lead to a smaller P_n than a $C < 0$ chirp, which makes the latter slightly preferable for the design.
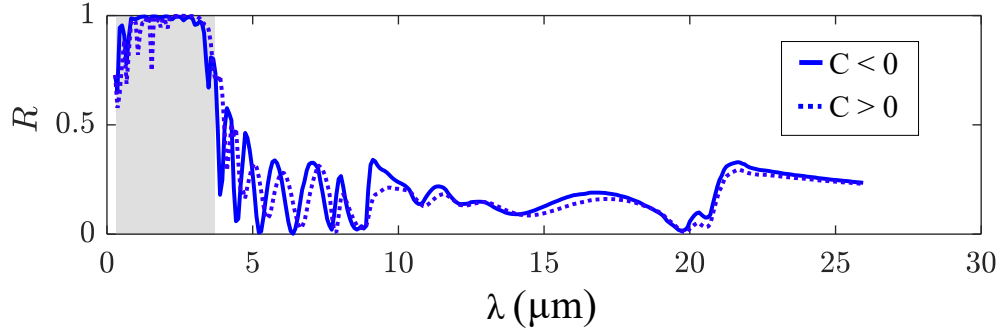
Fig. S5. Simulation results for a negative ($C < 0$) linearly chirped ML (solid blue curve), for a positive ($C > 0$) chirped ML (dotted blue curve), as those from the main text, with $N = 15$ and $\lambda_1 = 3.1$ µm. The targeted reflected BW covering the solar window is highlighted (grey shadow).

4. REFLECTANCE AND TRANSMITANCE FOR $\theta > 0°$

As explained in the manuscript, the net cooling power P_n is calculated from the absorbance (A) curves at several incidence angles θ, from the normal direction (0°) to 80°. Fig. S6 shows colormaps for $R(\lambda)$ and $T(\lambda)$ for several θ, from 0° to 80° in steps of 1° in the linearly chirped ML from the main text, with $N = 11$ and $\lambda_1 = 2.1$ µm. Note that $A = 1 - R$. We note a periodical dependence of R with θ, as naturally expected from the angular dependence of Fresnel equations, which can be easily found in any Optics dedicated book. Also, other high-R values are observed out of the targeted BW which, as discussed before, is caused mostly by interference of multiple Fresnel reflections in the chirped ML and on the substrate interface. A quantitative analysis of the

6
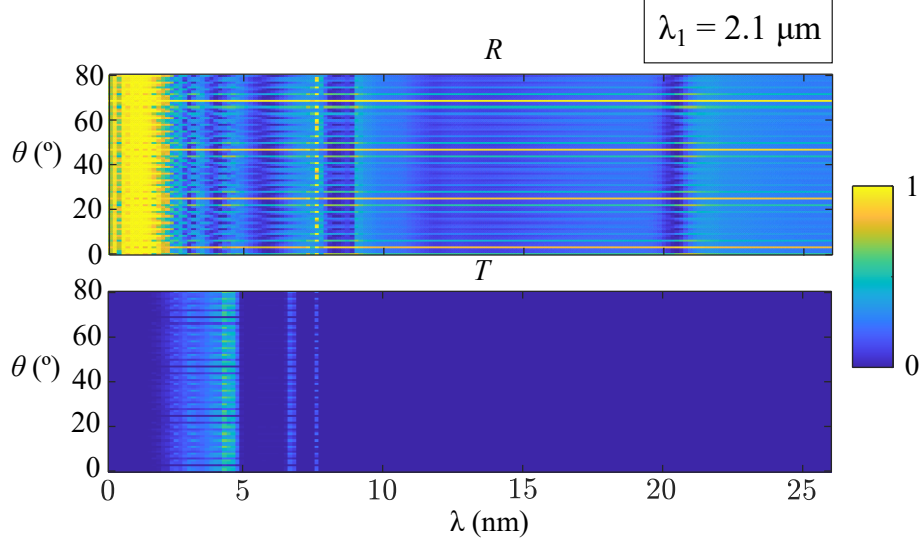
Fig. S6. Simulated reflectance (*R*) and transmittance (*T*) as functions of λ (up to 30 μm) and θ from $\theta = 0°$ to $\theta = 80°$ in steps of 1°, for $\lambda_1 = 2.1$ μm.

former phenomena is out of the scope of this section. On the other hand, *T* is clearly minimised in the explored range of λ and the targeted BW (i.e., yellow area between 0.3 μm and λ_1) is efficiently reflected for every θ.

5. ALGORITHM FOR A PROPORTIONAL DISTRIBUTION OF *N* SECTIONS FROM A DISCRETISED $I(\lambda_k)$

In section C in the main text, results from an ML with a distribution of *N* sections adapted to $I(\lambda)$ were shown. To efficiently build such ML, the proposed algorithm is the following: Firstly, the 'adapted chirping' function is obtained from modeling the solar irradiance curve with the black body radiation equation as in Fig. S4.

The number of sections in the grating devoted to reflect each Bragg wavelength λ_k is variable (n_k), adapted to the solar irradiance intensity at that frequency. In other words, the solar radiance curve is normalised to its maximum, discretised in $k - 1$ intervals ($I(\lambda_k)$), and the number of sections (n_k) for each λ_k is proportional to $I(\lambda_k)$. Mathematically,

$$n_k = N \frac{I(\lambda_k)}{\sum I(\lambda_k)} \tag{S3}$$

since $\sum n_k = N$. This way, the majority of sections in the grating will be concentrated in the most intense region of *I*, devoted to reflect the most intense wavelengths from *I*. Fig. S7(a) shows $I(\lambda)$ accordingly discretised, assuming a 'point' step-size that depends on the slope of the irradiance curve (the greater the slope, the smaller the step-size). We perform the discretisation of the curve with different step-sizes in three different wavelength intervals (see vertical dashed lines in Fig. S7(a)): Step-size of 0.075 μm for 0.28 μm $< \lambda \leq 0.4$ μm; 0.15 μm for 0.4 μm $< \lambda \leq 1.7$ μm; and 0.75 μm for 1.7 μm $< \lambda \leq 4$ μm. Hence, more λ_k are obtained around the high-intensity values of *I* (more pronounced slope) than in the outer regions. This can be regarded as a finer 'sampling' in the area of interest, where *I* is larger. We acknowledge there is some arbitrariness in choosing the step-size and the wavelength intervals as it clearly depends on the curve profile, which makes this particular step in the process difficult to generalise. However, the found interval central wavelengths adjust very well with those λ where the variation in the slope is minimal (i.e. second derivative of I_{bb} is minimal).

Fig. S7(b-e) show the number of sections (n_k) allocated for each λ_k for different values of *N*, in a proportional manner according to *I*. All results show that the long-wavelength regions in *I* can be disregarded ($n_k = 0$). This is reasonable given the lower *I* at such frequencies. We want to stress again that there is some arbitrariness in the number of sections obtained at certain wavelengths, as they also depend on the discretisation step-size of $I(\lambda)$. Discretised results however resemble

7
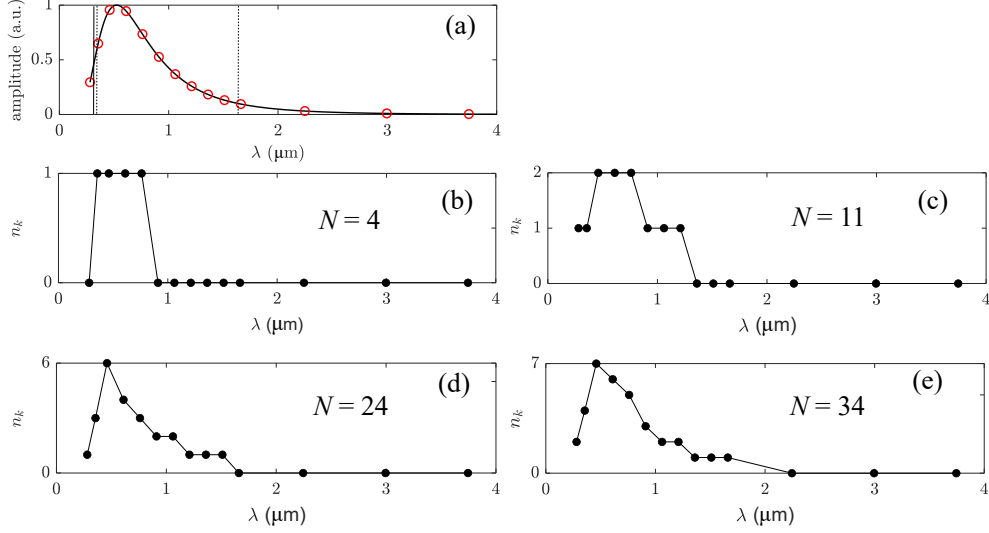
Fig. S7. (a) Normalised I modeled as a black body radiation curve at $T = 5778$ K, discretised in 14 λ_k (open red circles), or equivalently 13 intervals (indicated by the vertical lines), from a 'sampling' process dependent on the curve profile: The 'sampling frequency' or step-size is variable depending on the λ 'region' (see related text). (b-e) The number of sections n_k for each λ_k depends on the number of total sections (N) making the ML.

very well to $I(\lambda)$ with increasing N. For $N = 4$ (the smallest value), the distribution of sections leads to a linear chirping (one section per λ_k) but also to a strong truncation of the thickest sections (long λ_k). $N = 11$ also leads to a quasi-linear chirp, but adds only one more section to each three central λ_k in the spectra. For larger N, the linear chirping is lost and many sections are repeated for each λ_k. The effects of these various distributions of sections on R is discussed in more detail in the main text.

REFERENCES

1. Z. M. Zhang and C. J. Fu, "Unusual photon tunneling in the presence of a layer with a negative refractive index," Appl. Phys. Lett. **80**, 1097–1099 (2002).
2. G. Reed, "Device physics - the optical age of silicon," Nature **427**, 595–6 (2004).
3. F. X. Kaertner, H. Byun, F. Grawert, J. Gopinath, H. Shen, E. Ippen, S. Akiyama, J. Liu, K. Wada, and K. K. Lionel, "Silicon-germanium saturable absorber mirrors for ultra-short pulse generation," ECS Transactions **3**, 759 (2006).
4. M. Emsley, O. Dosunmu, and M. Unlu, "High-speed resonant-cavity-enhanced silicon pho-todetectors on reflecting silicon-on-insulator substrates," IEEE Photonics Technol. Lett. **14**, 519–521 (2002).
5. X. Yang, H. Li, W. Zhang, L. You, L. Zhang, X. Liu, Z. Wang, W. Peng, X. Xie, and M. Jiang, "Superconducting nanowire single photon detector with on-chip bandpass filter," Opt. Express **22**, 16267–16272 (2014).
6. K. Muro and K. Shiraishi, "Poly-Si/SiO/sub 2/ laminated walk-off polarizer having a beam-splitting angle of more than 20," J. Light. Technol. **16**, 127–133 (1998).
7. N. D. Gupta and V. Janyani, "Analysis of photonic crystal diffraction grating based light trapping structure for gaas solar cell," IETE J. Res. **67**, 714–725 (2021).
8. M. Ohring, *Materials Science of Thin Films: Depositon and Structure.* (Elsevier, 2001).
9. M. Cho, J.-H. Seo, D. Zhao, J. Lee, K. Xiong, X. Yin, Y. Liu, S.-C. Liu, M. Kim, T. J. Kim, X. Wang, W. Zhou, and Z. Ma, "Amorphous Si/SiO2 distributed Bragg reflectors with transfer printed single-crystalline Si nanomembranes," J. Vac. Sci. & Technol. B **34**, 040601 (2016).
10. T. Pilvi, T. Hatanpää, E. Puukilainen, K. Arstila, M. Bischoff, U. Kaiser, N. Kaiser, M. Leskelä, and M. Ritala, "Study of a novel ald process for depositing MgF2 thin films," J. Mater. Chem. **17(48)**, 5077–5083 (2007).
11. R. Thielsch, J. Heber, H. Uhlig, and N. Kaiser, "Development of mechanical stress in fluoride

multilayers for UV applications," in *Advances in Optical Thin Films,* vol. 5250 C. Amra, N. Kaiser, and H. A. Macleod, eds., International Society for Optics and Photonics (SPIE, 2004), pp. 127 – 136.

12. P. López-Reyes, B. Perea-Abarca, C. Honrado-Benítez, N. Gutiérrez-Luna, Álvaro Ríos-Fernández, L. V. R. de Marcos, and J. I. Larruquert, "Optimization of the deposition parameters of MgF2/LaF3 narrowband reflective FUV multilayers," Opt. Mater. Express **11**, 1678–1691 (2021).

13. "Gemini observatory, atmospheric transmittance spectra," https://www.gemini.edu/sciops/telescopes-and-sites/observing-condition-constraints/ir-transmission-spectra.

14. "Nrel, solar irradiance spectra," http://www.nrel.gov/grid/solar-resource/spectra-am1.5.html.

15. R. Kashyap, "Fiber bragg gratings 2nd edn," (Academic Press, Burlington, 2009), chap. Chirped Fiber Bragg Gratings.